Leading edge stability in motile cells is an emergent property of branched actin network growth

Rikki M. Garner[1,2] and Julie A. Theriot[2]*

[1]Biophysics Program, Stanford University School of Medicine, Stanford, CA, USA

[2]Department of Biology and Howard Hughes Medical Institute, University of Washington, Seattle, WA, USA

*Correspondence to: jtheriot@uw.edu

One sentence summary: An experimental and computational investigation of fluctuation dynamics at the leading edge of motile cells demonstrates that the specific angular geometry of Arp2/3-mediated actin network branch formation lies at the core of a successful biological noise-suppression strategy.

Abstract: Animal cell migration is predominantly driven by the coordinated, yet stochastic, polymerization of thousands of nanometer-scale actin filaments across micron-scale cell leading edges. It remains unclear how such inherently noisy processes generate robust cellular behavior. We employed high-speed, high-resolution imaging of migrating neutrophil-like HL-60 cells to explore the fine-scale dynamic shape fluctuations that emerge and relax throughout the process of leading edge maintenance. We then developed a minimal stochastic model of the leading edge that is able to reproduce this stable relaxation behavior. Remarkably, we find that lamellipodial stability *naturally emerges* from the interplay between branched actin network growth and leading edge shape – with no additional feedback required – based on a synergy between membrane-proximal branching and lateral spreading of filaments. These results thus demonstrate a novel biological noise-suppression mechanism based entirely on system geometry. Furthermore, our model suggests that the Arp2/3-mediated ~70-80º branching angle optimally smooths lamellipodial shape, addressing its long-mysterious conservation from protists to mammals.

Main text:

Cell migration driven by actin polymerization plays an essential role in countless organisms spanning the eukaryotic tree of life (*1*, *2*). Across this broad phylogeny, cells have been observed to form a dizzying array of protrusive actin structures, each exhibiting unique physical and biological properties (*3*). In all cases, the fundamental molecular unit of these micron-scale structures is the single actin filament, which polymerizes stochastically by addition of single monomers to push the leading edge membrane forward (*4–7*). Higher-order actin structures, and the biological functions they robustly enable, are therefore mediated by the collective action of thousands of stochastically growing filaments (*8*). It remains an open question how cells control for – or leverage – this inherent stochasticity to maintain stable leading edge protrusions over length and time scales more than three orders of magnitude larger than the scales of actin monomer addition (*9*, *10*).

Perhaps the archetype of dynamically stable actin structures is the lamellipodium, a flat "leaf-like" protrusion that is ~200 nm tall, up to 100 µm wide, and filled with a dense network of dendritically branched actin filaments (*11–14*). Cell types that undergo lamellipodial migration (most notably fish epidermal keratocytes and vertebrate neutrophils) can maintain a single, stable lamellipodium for minutes to hours, allowing the cells to carry out their biological functions (*15*, *16*). For example, in their *in vivo* role as first responders of the innate immune system, neutrophils must undergo persistent migration over millimeter-scale distances to reach sites of inflammation and infection (*17*, *18*). Regardless of the cell type, the origins of this striking stability in the face of stochastic actin filament polymerization remain elusive. The stability of lamellipodia has been theoretically proposed to depend on the dendritically branched structure of their actin networks, wherein filaments are oriented at an angle relative to the local membrane normal, allowing growing filament tips to spread out laterally along the leading edge as they polymerize (*16*, *19*). (Although any acute angle would permit spreading, we note that filament orientation in cells has been experimentally observed to be highly stereotyped, averaging ±35° relative to the

37 membrane normal (*20*, *21*) – approximately one half of the highly evolutionarily-conserved ~70º branch
38 angle mediated by the Arp2/3 complex (*22–24*).) Experimental efforts have further identified a number of
39 additional potential contributors to lamellipodial stability, including membrane tension (*25–29*), plasma
40 membrane curvature-sensing proteins (*29*), and force-feedback via directional filament branching (*30*).

41 Seeking to dissect the origins of lamellipodial stability, we pursued complimentary experimental
42 and computational methodologies. First, we performed high-speed, high-resolution microscopy on
43 migrating human neutrophil-like HL-60 cells to monitor their leading edge shape dynamics. In contrast to
44 the remarkable overall lamellipodial stability observed over minutes, high-speed imaging revealed that
45 the leading edge shape is extremely dynamic at shorter time and length scales, constantly undergoing fine-
46 scale fluctuations around the average cell shape. We determined that these shape fluctuations continually
47 dissipate (thereby enabling long time scale lamellipodial maintenance) in a manner quantitatively
48 consistent with viscous relaxation back to the time-averaged leading edge shape. We next developed a
49 minimal stochastic model of branched actin network growth against a flexible membrane, broadly
50 applicable to a wide variety of cell types, that was able to recapitulate the global leading edge stability and
51 fine-scale fluctuation relaxation behavior observed in cells. Our model suggests that the suppression of
52 stochastic fluctuations is an intrinsic, emergent property of collective actin dynamics at the leading edge,
53 as branched network geometry *alone* is necessary and sufficient to generate lamellipodial stability.
54 Moreover, we find that the evolutionarily-conserved geometry, the ~70° branching angle of the Arp2/3
55 complex, optimally quells shape fluctuations.

56

57 **Fine-scale leading edge shape fluctuations revealed at high spatiotemporal resolution**

58 Neutrophils form lamellipodia that are intrinsically lamellar, maintaining a thin, locally flat sheet of actin
59 even in the absence of support structures like the substrate surface (*14*). Here, we study the migration of

60 neutrophil-like HL-60 cells (*31*) within quasi-two-dimensional confinement between a glass coverslip and
61 an agarose pad overlay (*32*). In addition to serving as an excellent *in vitro* model for neutrophil
62 surveillance of tissues, this assay allows for easy visualization and quantification of lamellipodial
63 dynamics by restraining the lamellipodium to a single imaging plane. Cells in this type of confinement
64 can migrate persistently, maintaining nearly-constant cell shape, for time scales on the order of minutes
65 to hours (*15*, *33*). In order to capture leading edge dynamics on time scales more relevant to the stochastic
66 growth of individual filaments, we performed high-speed (20 Hz) imaging of migrating HL-60 cells.
67 These experiments revealed dynamic, fine-scale fluctuations around the average leading edge shape
68 (Fig. 1A, Movie S1, Fig. S1-S2, *Materials and Methods*), reminiscent of an excitable system in which
69 local instabilities in the leading edge emerge, grow, and then relax. Consistent with the idea that these
70 fluctuations arise from stochasticity in actin growth, kymograph analysis of curvature and velocity
71 (Fig. 1B-C) showed that relatively long-lived curvature fluctuations are formed by the continual
72 time-integration of very short-lived (sub-second, sub-micron) velocity fluctuations. Because the average
73 cell shape remains constant over time, there must be some form of feedback acting on leading edge
74 curvature to sustain stable lamellipodial growth. These rich, measurable fine-scale dynamics therefore
75 provide a unique opportunity to directly observe the time-evolution of leading edge maintenance. Taking
76 advantage of our high-precision measurements, we aimed to quantitatively investigate the properties of
77 the observed fluctuations, with the goal of determining the mechanisms by which molecular machinery at
78 the leading edge coordinates the stochastic polymerization of individual actin filaments.
79

80 **Lamellipodial stability mediated by viscous relaxation of shape fluctuations**

81 The relaxation of fine-scale shape fluctuations back to the steady-state leading edge shape is essential for
82 the long time scale stability of lamellipodia. As for any physical system, the nature of this relaxation

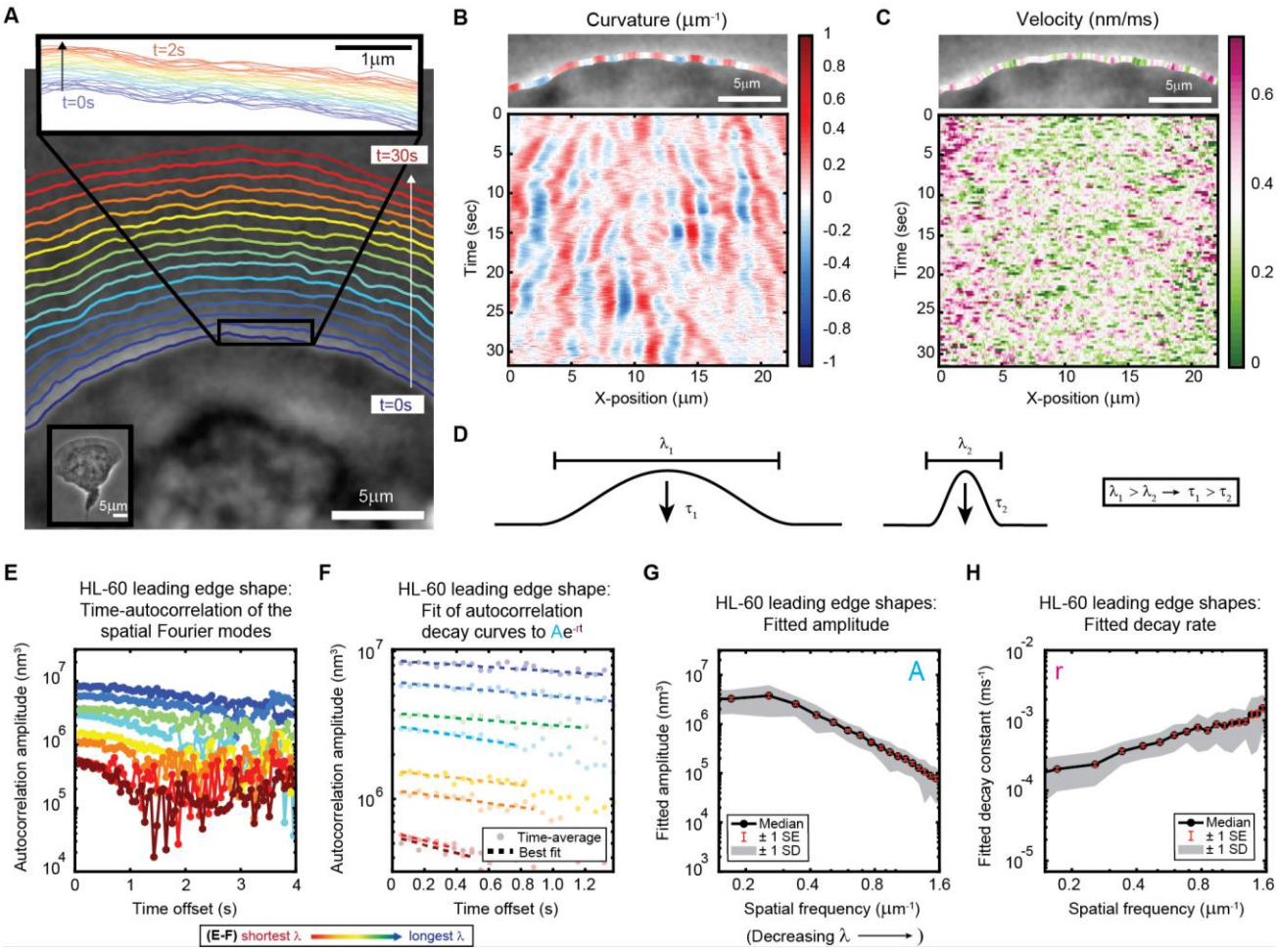

Fig. 1. High-speed, high-resolution imaging reveals fine-scale fluctuations in leading edge shape. (**A-C**) Example of leading edge fluctuations extracted from a representative migrating HL-60 cell. (A) Phase contrast microscopy image from the first frame of a movie, overlaid with segmented leading edge shapes from time points increasing from blue to red in 2 sec intervals. Top Inset: Magnification of the segmented leading edge between t = 0-2 sec increasing from blue to red in 50 ms intervals. Bottom Inset: A de-magnified image of the whole cell at the last time point. (B-C) Kymographs of curvature (B) and velocity (C). (**D**) Schematic demonstrating a commonly observed trend between fluctuation wavelength and relaxation time. (**E**) Autocorrelation amplitude (complex magnitude) of the spatial Fourier transform plotted as a function of time offset from a representative video of a cell. (**F**) Best fit of the autocorrelation data shown in (E) to an exponential decay, fitted out to a drop in amplitude of 2/*e*. (**G-H**) Fitted parameters of the autocorrelation averaged over 67 cells.

reflects the system's underlying physical properties; in this case, the characteristics of – and interactions between – actin filaments and the membrane. To provide a framework for exploration of the physical mechanisms underlying stable lamellipodial protrusion, we quantified the relaxation dynamics by performing time-autocorrelation analysis on the leading edge shape (*Materials and Methods*). Applied in

87 this context, this analytical technique calculates the extent to which the lamellipodium contour loses
88 similarity with the shape at previous time points as fluctuations emerge and relax. As most material
89 systems (actively-driven or otherwise) exhibit relaxation behavior with a characteristic wavelength-
90 dependence (e.g., Fig. 1D), we performed Fourier decomposition on the leading edge shape to separate
91 out fluctuations at different length scales, and then performed autocorrelation analysis separately on each
92 Fourier mode.

93 This analysis revealed a monotonic relaxation of shape fluctuations at each wavelength
94 (Fig. 1E-F); the decay is well-fit by an exponential form (Fig. 1F), consistent with overdamped viscous
95 relaxation. A clear wavelength-dependence is observed, with shorter wavelengths decaying faster and
96 having smaller amplitudes (Fig. 1G-H). This general trend is shared by many physical systems with linear
97 elastic constraints, such as idealized membranes (*34*) and polymers (*35*) freely fluctuating under Brownian
98 motion, but can be contrasted with systems that have a dominant wavelength, as in the case of buckling
99 or wrinkling of materials under compression (*36*).

100

101 **Leading edge stability as an emergent property of branched actin growth**

102 The rich behavior and quantitative nature of our leading edge shape fluctuation data made them ideal for
103 comparison with physical models. In order to determine the biophysical mechanisms underlying the
104 observed leading edge dynamics, we aimed to reproduce this behavior in a stochastic model of branched
105 actin network growth against a membrane (Fig. 2A-C, Movie S2, *Materials and Methods*). Previous
106 stochastic models of protrusive actin-based forces largely focused on actin polymerization against rigid
107 obstacles (e.g., the bacterial cell wall for the *Listeria* comet tail (*37*, *38*) or a single, flat membrane segment
108 in models of lamellipodia (*27*)). We expanded on this general framework to incorporate a two-dimensional
109 leading edge with filaments polymerizing against a flexible membrane, which is modeled as a system of

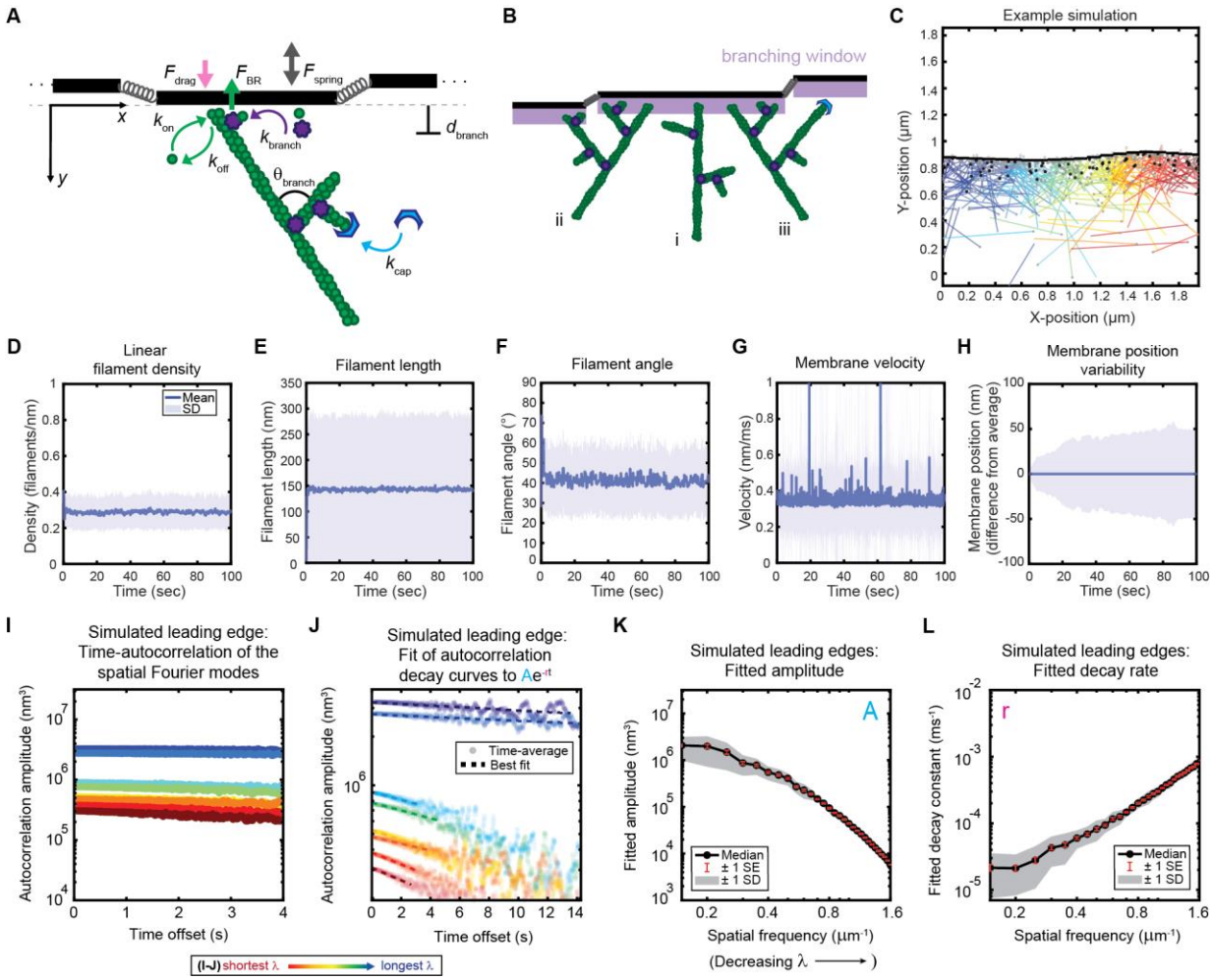

Fig. 2. Minimal model of branched actin growth recapitulates leading edge stability and shape fluctuation relaxation. (**A-B**) Model schematic. Black lines, membrane; green circles, actin; purple flowers, Arp2/3 complex; blue crescents, capping protein. Rates: k_{on}, polymerization; k_{off}, depolymerization; k_{branch}, branching; k_{cap}, capping. θ_{branch}, branching angle. d_{branch}, branching window. Physical parameters: F_{spring}, forces between membrane segments; F_{BR}, force of filaments on the membrane (Brownian ratchet); F_{drag}, viscous drag. (B) Schematic demonstrating filament angle evolution. Filaments growing perpendicular to the leading edge (i) outcompete their progeny (branches), leading to a reduction in filament density; filaments growing at an angle (ii and iii) make successful progeny. Filaments spreading down a membrane positional gradient (ii) are more evolutionarily successful than those spreading up (iii). (**C**) Simulation snapshot: Black lines, membrane; colored lines, filament equilibrium position and shape; gray dots, barbed ends; black dots, capped ends; filament color, x-position of membrane segment filament is pushing (increasing across the x-axis from blue to red). (**D-H**) For a representative simulation, mean (solid line) and standard deviation (shading) of various membrane and actin filament properties as a function of simulation time. Note for linear filament density (D) lamellipodia are ~10 filament stacks tall along the z-axis, giving mean filament spacing of 10/density ~ 30nm. (**I-L**) Autocorrelation analysis and fitting for a representative simulation (I-J) as well as best fit parameters averaged over 40 simulations (K-L).

110

membrane segments connected by springs. Simulated filaments apply force to the membrane following the classic untethered Brownian ratchet formalism (*4*), consistent with recent experiments showing that cellular protrusions are formed by largely untethered actin networks (*39*). Designed to be as comparable as possible to our experimental data, the model incorporated experimentally-measured values from the literature for the membrane tension, membrane bending modulus, and biochemical rate constants (Table S1-S2) (*4*, *40*). As we were specifically interested in identifying biophysical mechanisms regulating leading edge stability, we minimized the model's biological complexity by including only the core biochemical elements of actin network growth dynamics: polymerization, depolymerization, branching, and capping. All filament nucleation in the model occurs through dendritic branching (observed in cells to be mediated by the Arp2/3 complex, which catalyzes the nucleation of new "daughter" actin filaments as branches from the sides of pre-existing "mother" filaments at a characteristic angle of ~70º (*22–24*)). By simulating individual filament kinetics, the model captures the evolutionary dynamics of the filament network, allowing us to directly test hypothesized mechanisms for the interplay between actin network properties (e.g., filament orientation) and protrusion dynamics (*4*, *20*, *27*) (Fig. 2B).

To our great surprise, this very simple model was able to recapitulate stable leading edge fluctuations. Nascent leading edges reach steady state values for filament density, filament length, filament angle, membrane velocity, and (most importantly) membrane fluctuation amplitude within seconds, a biologically realistic time scale (Fig. 2D-H). Furthermore, the steady state values obtained are in quantitative agreement with both our own experimental data and previously published measurements, with the model yielding mean values of: 0.3 filaments/nm for filament density (~30 nm filament spacing for a lamellipodium that is 10 filaments tall (*12*)), ~150 nm for filament length, ~40° for filament angle (with respect to the membrane normal), ~0.35 nm/ms for membrane velocity, and ~50 nm for membrane fluctuation amplitude (*11*, *20*, *21*).

134 As observed in the experimental measurements, simulated leading edge shape stability is mediated
135 by an exponential decay of shape fluctuations (Fig. 2I-J). Furthermore, the minimal model correctly
136 predicts the monotonic trends of fluctuation amplitude and decay time scale with wavelength (Fig. 2K-L)
137 in a way that was not sensitive to our choices of simulation time step, membrane segment length, and
138 overall length of the leading edge (Fig. S3-5). It should be noted that the generation of the simulated data
139 in Figure 2K-L did not involve any curve-fitting (and therefore *no free parameters* that could be fit) to the
140 experimentally-measured autocorrelation dynamics. The simulated fluctuation relaxation behavior,
141 qualitatively reproducing our experimental measurements, emerges directly from the molecular-scale
142 actin growth model, in which all biochemical parameters were estimated from measurements in the
143 existing literature (Table S1-S2) – leaving no free simulation parameters.
144

145 **Predicting effects of drug treatment with Latrunculin B**

146 We were interested in further assaying the predictive power of this minimal stochastic model. As an
147 example, we elected to test whether the model could correctly predict the response of HL-60 cells to
148 treatment with the drug Latrunculin B, which binds to and sequesters actin monomers. Qualitatively, cells
149 treated with Latrunculin B (Movie S3) present with enhanced bleb formation and more variable leading
150 edge shapes, in comparison with cells treated with a DMSO vehicle control (Movie S4). In our model,
151 addition of this drug can be simulated by reducing the free monomer concentration, which consequently
152 reduces both the polymerization rate and the branching rate. At low effective doses, subtle but measurable
153 changes to leading edge fluctuations were predicted: specifically, an increase in the amplitudes at large
154 wavelengths, and a decrease in the decay rates across all wavelengths (Fig 3A-B). Our experimental
155 results were consistent with these quantiative predictions; Latrunculin B-treated cells exhibited increased
156 fluctuation amplitudes and decreased fluctuation rates over the predicted ranges (Fig. 3C-D).

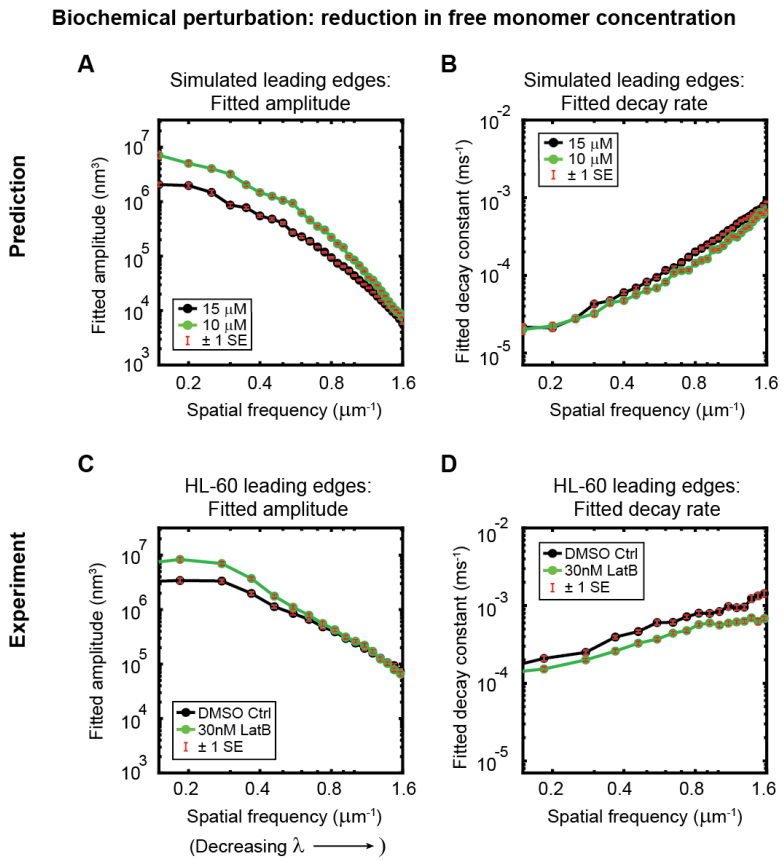

Fig. 3. Minimal model correctly predicts response of HL-60 cells to drug treatment. Predicted and experimentally-measured response of the autocorrelation decay fit parameters to drug treatment with Latrunculin B, plotted as in Fig. 1G-H. (**A-B**) Predicted response to a reduction in the free monomer concentration (green, 10 μM) compared to the standard concentration used in this work (black, 15 μM) – medians over 40 simulations for each condition. (**C-D**) Experimentally measured behavior: DMSO control – medians over 67 cells (same data as plotted in Fig. 1G-H). 30nM Latrunculin B – medians over 34 cells.

Geometry as the core determinant of simulated leading edge stability

Given the success of the model in reproducing experimental results, we next wanted to determine which features of the simulation were responsible for leading edge stability and relaxation of fluctuations. The simplicity of the model allowed us to determine the stability mechanism by process of elimination, selectively removing elements of the model (*Materials and Methods*) and determining whether stability was retained. Given that leading edge protrusion is resisted by a flexible membrane, we initially expected that shape fluctuations would be dominated by membrane tension or membrane bending rigidity. To assay the importance of these membrane properties, we removed the forces between the membrane segments (Fig. 2A, F_{spring}) from the simulation (*Materials and Methods*). Surprisingly, the coupling between the membrane segments (i.e., the effects of tension and bending at length scales larger than the size of an individual membrane segment) was completely dispensable for leading edge stability (Fig. 4A-E).

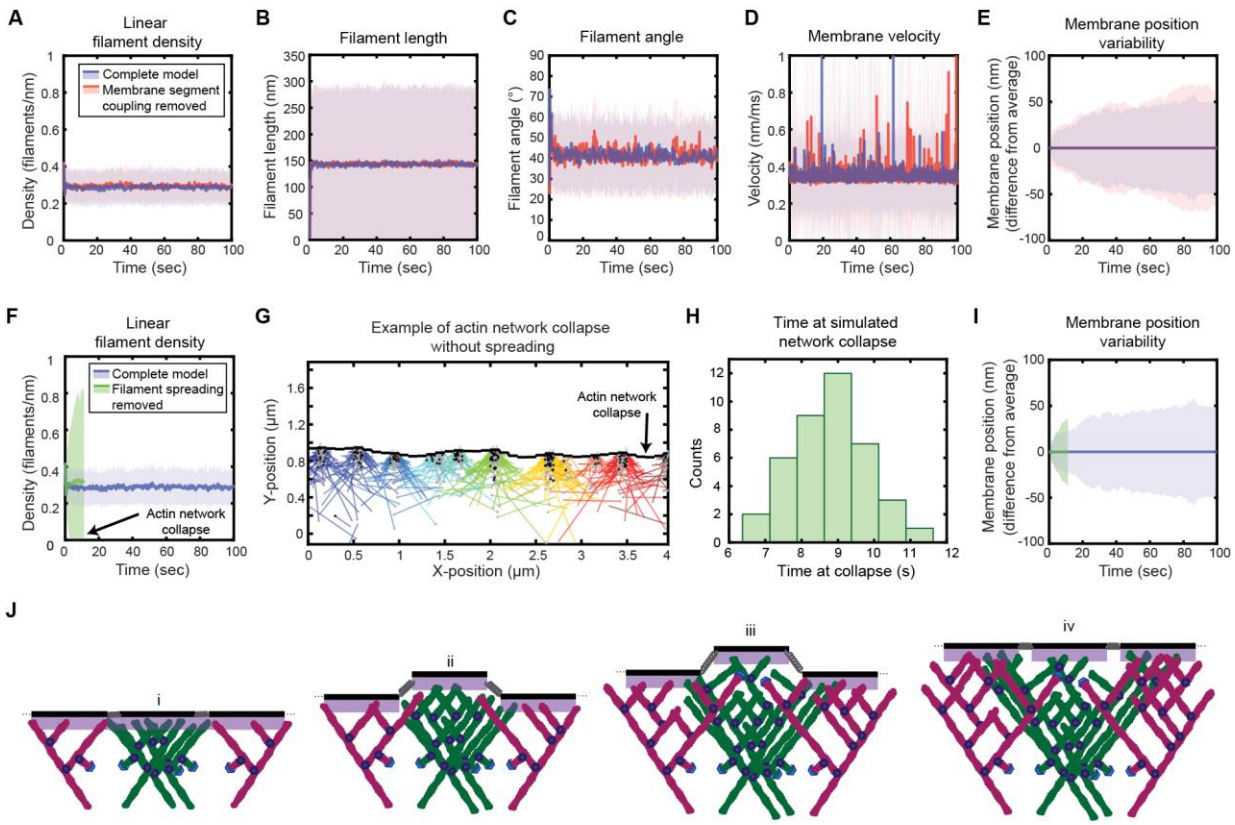

Fig. 4. Simulated lamellipodial stability is governed by leading edge geometry. (**A-E**) Comparison of leading edge properties with and without the coupling of the membrane segments by tension and bending rigidity (no coupling: F_{spring} = 0 in Fig. 2A), plotted as in Fig. 2D-H. (**F-I**) Comparison of leading edge properties with and without the ability of filaments to spread between neighboring membrane segments. (G) A snapshot of the simulation after filament network collapse (defined as a state where at least 25% of the membrane segments have no associated filaments). (F,G,I) Plots made from the same simulation. (H) A histogram of the average time to network collapse over 40 simulations. (**J**) Schematic representing the proposed molecular mechanism underlying the stability of leading edge shape, with time increasing from i-iv.

169 Following a similar process of elimination, we determined that in fact only two elements were required
170 for stability. First, as reported previously for dendritic actin network polymerization against a single stiff
171 obstacle, it was necessary to constrain branching to occur only within a fixed distance from the leading
172 edge membrane (Fig. 2A-B) in order to maintain a steady state actin density (*37*). The molecular
173 motivation for this spatially limited "branching window" is rooted in that fact that activators of the Arp2/3
174 complex, which render Arp2/3 competent for actin filament nucleation, are typically membrane-associated
175 proteins (*41*). Second, we found that stability is inherently tied to the ability of filaments to spread laterally

176 to neighboring membrane segments (Fig. 2B *ii-iii*, Fig. 4F-I). (Recall that, because the branched actin
177 network geometry causes filaments to grow, on average, at an angle relative to the membrane normal (*20*,
178 *21*), polymerizing tips spread laterally along the leading edge (*16*, *19*).) Removing filament spreading
179 from the model by fixing filaments to remain associated with their nearest membrane segment at birth
180 (*Materials and Methods*) led to actin density divergence: network regions with low filament density
181 eventually underwent complete depolymerization, while high-density regions continued to accumulate
182 actin (Fig. 4F-G).

183 These findings lead us to a simple molecular mechanism for leading edge stability, based on a
184 synergy between filament spreading and membrane-proximal branching (Fig. 4J): To begin with, regions
185 with initially high filament density come to protrude beyond the average position of the rest of the
186 membrane, representing the emergence of a leading edge shape fluctuation (Fig. 4J, *i-ii*). This induces
187 asymmetric filament spreading, where filaments from high-density regions can spread productively into
188 neighboring regions (Fig. 2B, *ii*), but filaments spreading from adjacent low-density regions cannot keep
189 up with the fast moving membrane segments (Fig. 2B, *iii*), and thus are unproductive (Fig. 4J, *ii-iii*). In
190 this way, the branched geometry inherent to dendritic actin polymerization, as well as its interaction with
191 the shape of the membrane, naturally encodes leading edge stability (Fig. 4J, *iv*). Thus our results directly
192 demonstrate a "stability-through-spreading" mechanism that has previously only been assumed in mean-
193 field analytical theories (*16*). Remarkably, this means that leading edge maintenance is an intrinsic,
194 emergent property of branched actin network growth against a membrane, without requiring any further
195 regulatory governance. Geometrical constraints imposed simply by the nature of membrane-proximal
196 actin branching ensure that any small variations in *either* local actin filament density *or* growth rate are
197 inherently self-correcting to regress toward the mean.

198 Of note, it has previously been shown that Arp2/3-mediated branching is required for lamellipodial
199 formation in a wide variety of cell types; cells with inhibited or depleted Arp2/3 complex exhibit complete
200 disruption of the lamellipodium shape and often switch to a different mode of migration altogether, such
201 as filopodial motility (*14*, *42*, *43*). Indeed, HL-60s treated with the Arp2/3 inhibitor CK-666 have
202 extremely variable leading edge shapes, characterized by long, thin filopodia-like protrusions (Movie S5).
203 Our theoretical results provide a mechanistic interpretation for this striking phenomenon, suggesting that
204 the vital lamellipodial maintenance role of Arp2/3-mediated branching stems from its ability to mediate
205 efficient filament spreading and equilibration of actin density fluctuations, purely because the daughter
206 filament always grows at an angle distinct from its mother.
207

208 **Optimal suppression of fluctuations by the highly-conserved ~70° branching angle**

209 Given the essential contribution of branched network geometry to the stability of the simulated leading
210 edges, we reasoned that variations in the branching geometry alone might have a significant effect on
211 leading edge fluctuations. We therefore performed simulations to determine the effects of changing the
212 average branching angle and branching angle variability on filament orientation, filament density, and
213 leading edge fluctuation fit parameters (Fig. 5). In this context, we highlight the distinction between the
214 branching angle, θ_{br} (i.e., the angle of a daughter filament relative to its mother), and the filament angle or
215 orientation, θ_f (i.e., the angle of a filament relative to the local membrane normal) (Fig. 5A, inset). In
216 effect, our simulations represent selection assays, as mother filaments compete to stay within the fixed
217 branching window, spawn daughter branches, and thus pass down their angle to their progeny (*20*). For
218 example, when filaments are initialized with a random orientation, and the branching angle is fixed (i.e.,
219 there is no variability in the branching angle), only a handful of mother filament angles (θ_f) survive until
220 the end of the simulation (Fig. 5A-C). The surviving, successful filament angles are narrowly and

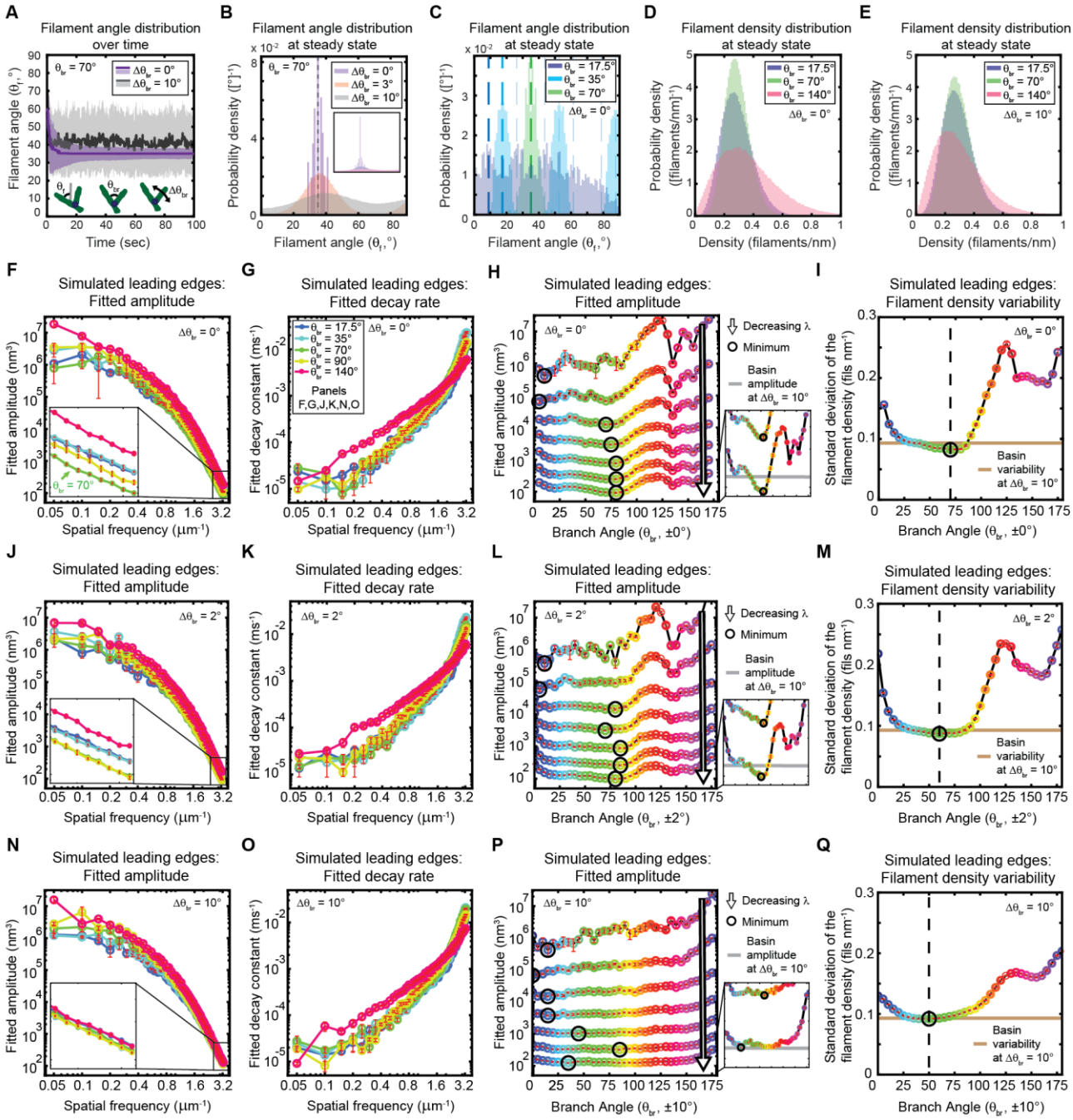

Fig. 5. The genetically-encoded Arp2/3-mediated branching angle is optimal for suppressing leading edge fluctuations. (**A-C**) Time course (A) and steady state distribution (B-C) of the filament angle (θ_f) for simulations with various branching angle standard deviations ($\Delta\theta_{br}$, A-B) and means (θ_{br}, C). Dashed lines represent $\theta_{br}/2$ plus integer multiples of θ_{br}. (**D-E**) Steady state filament density distribution as a function of the mean branching angle in the context of $\Delta\theta_{br}$=0˚ (D) and $\Delta\theta_{br}$=10˚ (E). (A-B, D-E) Results from a representative simulation for each condition. (C) Data integrated over 40 simulations. (**F-Q**) Predicted response of leading edge fluctuations and filament density variability to changes in the branch angle and branch angle variability, **(continued on next page)**

221

(Fig. 5 continued) medians over 40 simulations for each condition. Red error bars – standard error. Color map is identical for panels C-Q. (H,L,P) Fitted amplitude as a function of branch angle, where each line represents a different spatial frequency, increasing from 0.2-3.2 um^{-1} in intervals of 0.5 um^{-1}. Insets have identical x-axes to main panels. (I,M,Q) Standard deviation of the filament density at steady state plotted as a function of branch angle. Note the x- and y-axes limits in (F-G, J-K, N-O) are expanded compared to the equivalent panels in Figs. 1-3.

222 symmetrically distributed around one half of the branching angle (Fig. 5B-C). This optimal filament angle
223 allows mother and daughter filaments to branch back and forth symmetrically about the membrane normal,
224 such that mother filaments do not out-compete their progeny (Fig. 2B) (*20*).

225 In living cells, branching is mediated by the Arp2/3 complex, which has been experimentally
226 measured to form highly regular and sterotyped branches at ~70° (*22–24*). Intriguingly, this protein
227 complex is highly conserved (*44*), with measurements of the branching angle in a wide variety of species
228 (protists (*22–24*, *45*), yeast (*24*), mammals (*24*, *45*, *46*), and amphibians (*47*)) using various experimental
229 techniques (platinum replica electron microscopy, cryo-electron microscopy, and total internal reflection
230 microscopy) all falling within the range of 67-78° (± 2-13°). The high degree of conservation hints that
231 this specific angle might carry some functional optimality, but the question has not been addressable
232 experimentally; due to the lack of naturally occuring Arp2/3 variants with a substantially different
233 branching angle, an alternative branching structure would hypothetically have to be designed do novo,
234 presumably by altering the protein interaction interface by which the Arp2/3 complex binds to the side of
235 a mother filament (*23*). We thus sought to explore the possible functional significance of this conserved
236 angle using our minimal stochastic model. Excitingly, we found that in simulations with no branch angle
237 variability, a 70-80° branching angle was optimal for minimizing both actin density fluctuations
238 (Fig. 5D,I) and leading edge fluctuation amplitudes for wavelengths smaller than ~2 µm (Fig. 5F,H).
239 These results provide tantalizing mechanistic insight into the long-standing question of why this angle is
240 so ubiquitous.

241 Heritability of filament orientation (i.e., the extent to which mother filament orientation determines
242 the orientation of the daughters) is set by the degree of variability in the branching angle (which, in turn,
243 reflects the influence of thermal fluctuations). Perhaps unsurprisingly, decreasing this orientational
244 heritability significantly reduces the dependence of fluctuation amplitude and filament density variability
245 on the branching angle (Fig. 5J-Q), and thereby counteracts the beneficial effect of the optimal angle on
246 leading edge fluctuations. Introducing a branch angle variability of ±2° (on the lower end of the
247 experimentally-measured values) broadens the range of near-optimal branch angles but maintains the
248 optimum at ~70-80° (Fig. 5J,L), while introducing a variability of ±10° (on the higher end of the measured
249 range) completely removes the optimum (Fig. 5N,P). In both cases, increasing the branch angle variability
250 increases the minimum possible fluctuation amplitude (Fig. 5H,L,P – insets) and filament density
251 variability (Fig. 5I,M,Q), representing a decrease in the noise-suppression capabilities of the system.
252 Overall, these results provide strong support for the idea that actin network geometry is not only essential
253 for leading edge stability, but also plays a major role in determining the fundamental limits of smoothness
254 in lamellipodial shape.
255

256 **Discussion**

257 The emergence of robust collective behaviors from stochastic elements is an enduring biological mystery
258 which we are only beginning to unravel (*48–54*). The apparent dichotomy in actin-based motility between
259 the random elongation of individual filaments and the stable formation of smooth and persistent higher-
260 order actin structures such as lamellipodia exemplifies this enigma, and provides an avenue towards
261 understanding general strategies for noise suppression in biological systems.

262 In recent years it has become clear that perturbation-free experiments which examine fluctuations
263 around the mean at steady state (in contrast to probing the change in the mean due to a perturbation) can

be a powerful tool for understanding noisy systems (*55*). In this work, application of that principle in combination with high-precision measurements, quantitative analytical techniques, and physical modeling led to the surprising revelation that the suppression of stochastic fluctuations *naturally emerges* from the interactions between a growing actin network and the leading edge membrane, with *no additional feedback required*.

Cells migrating *in vivo* inevitably experience a much more challenging and dynamic environment, in which additional feedback mechanisms will almost certainly be required for the maintenance of polarized migration. The simplicity and biophysical realism of our modeling framework should make it particularly well-suited for future studies focused on predicting and understanding the effects of additional potential feedback mechanisms, including tethering (*56–59*), a limiting monomer concentration (*60*), force-dependent branching (*30*, *61*, *62*), and regulation by curvature-sensing proteins (*29*, *63*). Further, this computational model might be useful for exploring the effects of various extracellular forces, such as those produced by obstacles or variations in matrix density. We also note that a certain degree of biochemical signaling is implicit in our model in the form of biochemical rate constants that are invariant in time and space; this property relies on signaling networks to maintain uniform gradients of actin-associated molecules (*64*). How local biochemical control (or lack thereof) over these rate constants might affect leading edge fluctuations remains an interesting avenue for future investigation, both theoretically and experimentally.

The defining characteristic and major advance of our model was the explicit inclusion of both the evolutionary dynamics of the actin network and its interaction with the two-dimensional geometry of the leading edge. By selectively removing elements of the model, we determined that lateral filament spreading, combined with a fixed branching window, is indispensable for leading edge stability. This highlights the crucial role in lamellipodial maintenance of the branched structure of actin networks,

287 wherein each daughter filament inherits angular information from its mother. Our further investigations
288 into the evolutionary properties of actin network growth revealed that a ~70-80° branch angle maximally
289 suppresses fine-scale actin density and leading edge shape fluctuations, showing for the first time that
290 Arp2/3-mediated branching imparts optimal functionality, as was long hypothesized based on strong
291 sequence, structural, and functional conservation throughout the eukaryotic tree of life.

292 Returning to the broader question of how noisy biological systems control for stochasticity, we
293 find that stability in the case of lamellipodial dynamics is inherently encoded by the geometry of branched
294 actin network growth. It will be interesting to see whether similar principles hold for other cytoskeletal
295 structures with clear geometric constraints, such as endocytic pits, the cytokinetic ring, and the mitotic
296 spindle.

297 **References:**

298 1. T. D. Pollard, J. A. Cooper, Actin, a Central Player in Cell Shape and Movement. *Science*. **326**,
299 1208–1212 (2009).
300 2. L. K. Fritz-Laylin, S. J. Lord, R. D. Mullins, WASP and SCAR are evolutionarily conserved in
301 actin-filled pseudopod-based motility. *J. Cell Biol.* **216**, 1673–1688 (2017).
302 3. T. Svitkina, The actin cytoskeleton and actin-based motility. *Cold Spring Harb. Perspect. Biol.*
303 **10**, 1–21 (2018).
304 4. A. Mogilner, G. Oster, Cell motility driven by actin polymerization. *Biophys. J.* **71**, 3030–45
305 (1996).
306 5. C. S. Peskin, G. M. Odell, G. F. Oster, Cellular motions and thermal fluctuations: the Brownian
307 ratchet. *Biophys. J.* **65**, 316–324 (1993).
308 6. J. A. Theriot, T. J. Mitchison, L. G. Tilney, D. A. Portnoy, The rate of actin-based motility of
309 intracellular Listeria monocytogenes equals the rate of actin polymerization. *Nature*. **357**, 257–
310 260 (1992).
311 7. M. Prass, K. Jacobson, A. Mogilner, M. Radmacher, Direct measurement of the lamellipodial
312 protrusive force in a migrating cell. *J. Cell Biol.* **174**, 767–772 (2006).
313 8. T. M. Svitkina, Ultrastructure of protrusive actin filament arrays. *Curr. Opin. Cell Biol.* **25**, 574–
314 581 (2013).
315 9. S. M. Rafelski, J. A. Theriot, Crawling Toward a Unified Model of Cell Motility: Spatial and
316 Temporal Regulation of Actin Dynamics. *Annu. Rev. Biochem.* **73**, 209–239 (2004).
317 10. D. Vavylonis, Q. Yang, B. O'Shaughnessy, Actin polymerization kinetics, cap structure, and
318 fluctuations. *Proc. Natl. Acad. Sci. U. S. A.* **102**, 8543–8548 (2005).
319 11. T. M. Svitkina, A. B. Verkhovsky, K. M. McQuade, G. G. Borisy, Analysis of the actin-myosin II

320 system in fish epidermal keratocytes: Mechanism of cell body translocation. *J. Cell Biol.* **139**,
321 397–415 (1997).
322 12. V. C. Abraham, V. Krishnamurthi, D. L. Taylor, F. Lanni, The Actin-Based Nanomachine at the
323 Leading Edge of Migrating Cells. *Biophys. J.* **77**, 1721–1732 (1999).
324 13. V. M. Laurent, S. Kasas, A. Yersin, T. E. Schäffer, S. Catsicas, G. Dietler, A. B. Verkhovsky, J.-
325 J. Meister, Gradient of rigidity in the lamellipodia of migrating cells revealed by atomic force
326 microscopy. *Biophys. J.* **89**, 667–675 (2005).
327 14. L. K. Fritz-Laylin, M. Riel-Mehan, B.-C. Chen, S. J. Lord, T. D. Goddard, T. E. Ferrin, S. M.
328 Nicholson-Dykstra, H. Higgs, G. T. Johnson, E. Betzig, R. D. Mullins, Actin-based protrusions of
329 migrating neutrophils are intrinsically lamellar and facilitate direction changes. *Elife*. **6** (2017),
330 doi:10.7554/eLife.26990.
331 15. T. Y. C. Tsai, S. R. Collins, C. K. Chan, A. Hadjitheodorou, P.-Y. Lam, S. S. Lou, H. W. Yang, J.
332 Jorgensen, F. Ellett, D. Irimia, M. W. Davidson, R. S. Fischer, A. Huttenlocher, T. Meyer, J. E.
333 Ferrell, J. A. Theriot, Efficient Front-Rear Coupling in Neutrophil Chemotaxis by Dynamic
334 Myosin II Localization. *Dev. Cell*. **49**, 189–205 (2019).
335 16. C. I. Lacayo, Z. Pincus, M. M. VanDuijn, C. A. Wilson, D. A. Fletcher, F. B. Gertler, A.
336 Mogilner, J. A. Theriot, Emergence of Large-Scale Cell Morphology and Movement from Local
337 Actin Filament Growth Dynamics. *PLoS Biol.* **5**, 2035–2052 (2007).
338 17. S. De Oliveira, E. E. Rosowski, A. Huttenlocher, Neutrophil migration in infection and wound
339 repair: Going forward in reverse. *Nat. Rev. Immunol.* **16**, 378–391 (2016).
340 18. E. Kolaczkowska, P. Kubes, Neutrophil recruitment and function in health and inflammation. *Nat.
341 Rev. Immunol.* **13**, 159–175 (2013).
342 19. H. P. Grimm, A. B. Verkhovsky, A. Mogilner, J. J. Meister, Analysis of actin dynamics at the

343 leading edge of crawling cells: implications for the shape of keratocyte lamellipodia. *Eur.*
344 *Biophys. J.* **32**, 563–577 (2003).
345 20. I. V. Maly, G. G. Borisy, Self-organization of a propulsive actin network as an evolutionary
346 process. *Proc. Natl. Acad. Sci.* **98**, 11324–11329 (2001).
347 21. A. B. Verkhovsky, O. Y. Chaga, S. Schaub, T. M. Svitkina, J.-J. Meister, G. G. Borisy,
348 Orientational Order of the Lamellipodial Actin Network as Demonstrated in Living Motile Cells.
349 *Mol. Biol. Cell*. **14**, 2559–2569 (2003).
350 22. R. D. Mullins, J. A. Heuser, T. D. Pollard, The interaction of Arp2/3 complex with actin:
351 Nucleation, high affinity pointed end capping, and formation of branching networks of filaments.
352 *Proc. Natl. Acad. Sci.* **95**, 6181–6186 (1998).
353 23. N. Volkmann, K. J. Amann, S. Stoilova-McPhie, C. Egile, D. C. Winter, L. Hazelwood, J. E.
354 Heuser, R. Li, T. D. Pollard, D. Hanein, Structure of arp2/3 complex in its activated state and in
355 actin filament branch junctions. *Science*. **293**, 2456–2459 (2001).
356 24. I. Rouiller, X. P. Xu, K. J. Amann, C. Egile, S. Nickell, D. Nicastro, R. Li, T. D. Pollard, N.
357 Volkmann, D. Hanein, The structural basis of actin filament branching by the Arp2/3 complex. *J.*
358 *Cell Biol.* **180**, 887–895 (2008).
359 25. A. Diz-Muñoz, K. Thurley, S. Chintamen, S. J. Altschuler, L. F. Wu, D. A. Fletcher, O. D.
360 Weiner, Membrane Tension Acts Through PLD2 and mTORC2 to Limit Actin Network
361 Assembly During Neutrophil Migration. *PLOS Biol.* **14**, e1002474 (2016).
362 26. A. R. Houk, A. Jilkine, C. O. Mejean, R. Boltyanskiy, E. R. Dufresne, S. B. Angenent, S. J.
363 Altschuler, L. F. Wu, O. D. Weiner, Membrane tension maintains cell polarity by confining
364 signals to the leading edge during neutrophil migration. *Cell*. **148**, 175–188 (2012).
365 27. J. Mueller, G. Szep, M. Nemethova, I. de Vries, A. D. Lieber, C. Winkler, K. Kruse, J. V. Small,

366 C. Schmeiser, K. Keren, R. Hauschild, M. Sixt, Load Adaptation of Lamellipodial Actin
367 Networks. *Cell*. **171**, 188–200 (2017).
368 28. N. C. Gauthier, T. A. Masters, M. P. Sheetz, Mechanical feedback between membrane tension
369 and dynamics. *Trends Cell Biol.* **22**, 527–535 (2012).
370 29. K. Tsujita, T. Takenawa, T. Itoh, Feedback regulation between plasma membrane tension and
371 membrane-bending proteins organizes cell polarity during leading edge formation. *Nat. Cell Biol.*
372 **17**, 749–758 (2015).
373 30. V. I. Risca, E. B. Wang, O. Chaudhuri, J. J. Chia, P. L. Geissler, D. a. Fletcher, Actin filament
374 curvature biases branching direction. *Proc. Natl. Acad. Sci.* **109**, 2913–2918 (2012).
375 31. B. J. Spellberg, M. Collins, S. W. French, J. E. Edwards, Y. Fu, A. S. Ibrahim, A phagocytic cell
376 line markedly improves survival of infected neutropenic mice. *J. Leukoc. Biol.* **78**, 338–344
377 (2005).
378 32. A. Millius, O. D. Weiner, in *Chemotaxis* (Humana Press, Totowa, NJ, 2009;
379 http://link.springer.com/10.1007/978-1-60761-198-1_11), vol. 571, pp. 167–177.
380 33. Neutrophil-like HL-60 cells expressing only GFP-tagged β-actin exhibit nearly normal motility,
381 doi:https://doi.org/10.1002/cm.21603.
382 34. F. L. H. Brown, Elastic Modeling of Biomembranes and Lipid Bilayers. *Annu. Rev. Phys. Chem.*
383 **59**, 685–712 (2008).
384 35. P. G. De Gennes, Dynamics of Entangled Polymer Solutions. I. The Rouse Model.
385 *Macromolecules*. **9**, 587–593 (1976).
386 36. E. Cerda, L. Mahadevan, Geometry and Physics of Wrinkling. *Phys. Rev. Lett.* **90**, 074302
387 (2003).
388 37. A. E. Carlsson, Growth of Branched Actin Networks against Obstacles. *Biophys. J.* **81**, 1907–

389 1923 (2001).

390 38. A. E. Carlsson, Growth Velocities of Branched Actin Networks. *Biophys. J.* **84**, 2907–2918
391 (2003).

392 39. A. Bisaria, A. Hayer, D. Garbett, D. Cohen, T. Meyer, Membrane-proximal F-actin restricts local
393 membrane protrusions and directs cell migration. *Science*. **368**, 1205–1210 (2020).

394 40. A. D. Lieber, S. Yehudai-Resheff, E. L. Barnhart, J. A. Theriot, K. Keren, Membrane tension in
395 rapidly moving cells is determined by cytoskeletal forces. *Curr. Biol.* **23**, 1409–1417 (2013).

396 41. S. Suetsugu, Activation of nucleation promoting factors for directional actin filament elongation:
397 Allosteric regulation and multimerization on the membrane. *Semin. Cell Dev. Biol.* **24**, 267–271
398 (2013).

399 42. J. H. Henson, M. Yeterian, R. M. Weeks, a. E. Medrano, B. L. Brown, H. L. Geist, M. D. Pais, R.
400 Oldenbourg, C. B. Shuster, Arp2/3 Complex Inhibition Radically Alters Lamellipodial Actin
401 Architecture, Suspended Cell Shape, and the Cell Spreading Process. *Mol. Biol. Cell*. **26** (2015),
402 doi:10.1091/mbc.E14-07-1244.

403 43. C. Wu, S. B. Asokan, M. E. Berginski, E. M. Haynes, N. E. Sharpless, J. D. Griffith, S. M.
404 Gomez, J. E. Bear, Arp2/3 is critical for lamellipodia and response to extracellular matrix cues
405 but is dispensable for chemotaxis. *Cell*. **148**, 973–987 (2012).

406 44. M. D. Welch, A. H. Depace, S. Verma, A. Iwamatsu, T. J. Mitchison, The Human Arp2/3
407 Complex Is Composed of Evolutionarily Conserved Subunits and Is Localized to Cellular
408 Regions of Dynamic Actin Filament Assembly. *J. Cell Biol.* **138**, 375–384 (1997).

409 45. L. Blanchoin, K. J. Amann, H. N. Higgs, J. Marchand, D. A. Kaiser, T. D. Pollard, Direct
410 observation of dendritic actin filament networks nucleated by Arp2/3 complex and WASP/Scar
411 proteins. *Nature*. **404**, 1007–1011 (2000).

412 46. L. Cai, A. M. Makhov, D. A. Schafer, J. E. Bear, Coronin 1B antagonizes cortactin and remodels
413 Arp2/3-containing actin branches in lamellipodia. *Cell*. **134**, 828–842 (2008).
414 47. T. M. Svitkina, G. G. Borisy, Arp2/3 complex and actin depolymerizing factor/cofilin in dendritic
415 organization and treadmilling of actin filament array in lamellipodia. *J. Cell Biol.* **145**, 1009–1026
416 (1999).
417 48. W. Y. C. Huang, Q. Yan, W. C. Lin, J. K. Chung, S. D. Hansen, S. M. Christensen, H. L. Tu, J.
418 Kuriyan, J. T. Groves, Phosphotyrosine-mediated LAT assembly on membranes drives kinetic
419 bifurcation in recruitment dynamics of the Ras activator SOS. *Proc. Natl. Acad. Sci.* **113**, 8218–
420 8223 (2016).
421 49. N. Battich, T. Stoeger, L. Pelkmans, Control of Transcript Variability in Single Mammalian Cells.
422 *Cell*. **163**, 1596–1610 (2015).
423 50. A. Y. Chang, W. F. Marshall, Organelles - Understanding noise and heterogeneity in cell biology
424 at an intermediate scale. *J. Cell Sci.* **130**, 819–826 (2017).
425 51. L. Mohapatra, B. L. Goode, P. Jelenkovic, R. Phillips, J. Kondev, Design Principles of Length
426 Control of Cytoskeletal Structures. *Annu. Rev. Biophys.* **45**, 85–116 (2016).
427 52. A. Raj, A. van Oudenaarden, Nature, Nurture, or Chance: Stochastic Gene Expression and Its
428 Consequences. *Cell*. **135**, 216–226 (2008).
429 53. W. T. Gray, S. K. Govers, Y. Xiang, B. R. Parry, M. Campos, S. Kim, C. Jacobs-Wagner,
430 Nucleoid Size Scaling and Intracellular Organization of Translation across Bacteria. *Cell*. **177**,
431 1632-1648.e20 (2019).
432 54. A. C. Oates, What's all the noise about developmental stochasticity? *Development*. **138**, 601–607
433 (2011).
434 55. E. S. Welf, G. Danuser, Using fluctuation analysis to establish causal relations between cellular

435 events without experimental perturbation. *Biophys. J.* **107**, 2492–2498 (2014).

436 56. A. Mogilner, G. Oster, Force generation by actin polymerization II: The elastic ratchet and
437 tethered filaments. *Biophys. J.* **84**, 1591–1605 (2003).

438 57. F. S. Soo, J. A. Theriot, Adhesion controls bacterial actin polymerization-based movement. *Proc.*
439 *Natl. Acad. Sci.* **102**, 16233–16238 (2005).

440 58. J. B. Alberts, G. M. Odell, In silico reconstitution of Listeria propulsion exhibits nano-saltation.
441 *PLoS Biol.* **2** (2004), doi:10.1371/journal.pbio.0020412.

442 59. S. C. Kuo, J. L. McGrath, Steps and fluctuations of Listeria monocytogenes during actin-based
443 motility. *Nature*. **407**, 1026–1029 (2000).

444 60. R. D. Mullins, P. Bieling, D. A. Fletcher, From solution to surface to filament: actin flux into
445 branched networks. *Biophys. Rev.* **10**, 1537–1551 (2018).

446 61. O. Chaudhuri, S. H. Parekh, D. A. Fletcher, Reversible stress softening of actin networks. *Nature*.
447 **445**, 295–298 (2007).

448 62. S. H. Parekh, O. Chaudhuri, J. A. Theriot, D. A. Fletcher, Loading history determines the velocity
449 of actin-network growth. *Nat. Cell Biol.* **7**, 1219–1223 (2005).

450 63. H. Zhao, A. Pykäläinen, P. Lappalainen, I-BAR domain proteins: linking actin and plasma
451 membrane dynamics. *Curr. Opin. Cell Biol.* **23**, 14–21 (2011).

452 64. P. N. Devreotes, S. Bhattacharya, M. Edwards, P. A. Iglesias, T. Lampert, Y. Miao, Excitable
453 Signal Transduction Networks in Directed Cell Migration. *Annu. Rev. Cell Dev. Biol.* **33**, 103–
454 125 (2017).

455

Acknowledgements:

We kindly thank E. F. Koslover and A. J. Spakowitz for their helpful advice on model conceptualization and data analysis, and E. F. Koslover, N. M. Belliveau, P. Radhakrishnan, and A. Savinov for helpful comments on the manuscript. Funding: Howard Hughes Medical Institute, Washington Research Foundation, NIH Grant R37-AI036929 to J.A.T., Gerald J. Lieberman Fellowship to R.M.G, NSF Graduate Research Fellowship to R.M.G.

Author contributions:

Study was conceived by R.M.G. and J.A.T. All experiments, modeling, and analysis were carried out by R.M.G. Interpretation of the results and preparation of the manuscript were performed by R.M.G. and J.A.T.

Competing Interests Statement:

The authors declare no competing financial interests.

Data and Materials Availability:

Analysis and modeling code for this paper is available on the Theriot lab Gitlab: <https://gitlab.com/theriot_lab/leading-edge-stability-in-motile-cells-is-an-emergent-property-of-branched-actin-network-growth>. All data will be made available upon reasonable request to the corresponding author.